JOURNAL OF GEOPHYSICAL RESEARCH, VOL. 106, NO. C10, PAGES 22,425–22,440, OCTOBER 15, 2001

Decadal deep-water variability in the subtropical Atlantic and convection in the Weddell Sea

Achim Stössel

Department of Oceanography, Texas A&M University, College Station, Texas, USA

Seong-Joong Kim

Canadian Center for Climate Modelling and Analysis, University of Victoria, Victoria, British Columbia, Canada

Abstract. This study suggests a link between convection in the Weddell Sea and deep-water flows in the (sub)tropical Atlantic. Employing a global sea ice–ocean general circulation model, events of enhanced convection are found to create enhanced outflow of Antarctic Bottom Water (AABW), the associated anomaly of which propagates rapidly along the model's deep western boundary. The propagation timescale of the order of a few years to reach the tropical Atlantic matches baroclinic Kelvin waves with phase speed corrected for the model's grid resolution. This feature is consistent with earlier findings on the baroclinic adjustment to perturbations of the rate of North Atlantic Deep Water (NADW) formation. The mean deep ocean transports, as well as the timescales and amplitudes of the deep ocean anomalies, are in good agreement with observation-based estimates. Upon arrival in the deep western tropical Atlantic, the model AABW anomalies induce strong anomalies in NADW outflow. This behavior suggests that the actual magnitude of NADW outflow across 30°S is highly susceptible to external perturbations on the baroclinic adjustment timescale. The implied higher susceptibility is supported by recent observations that NADW turns mostly eastward between 20°S and 30°S. The NADW anomalies eventually propagate southward and join the Antarctic Circumpolar Current. There is weak indication that the associated anomalies enter the eastern Weddell Gyre to eventually feed back on the critical convection site in the Weddell Sea, possibly sustaining the oscillation. However, there is stronger evidence that the anomalies initially created by the convective events are advected with the model's Weddell Gyre, the advective timescale of which (10–12 years) is consistent with the periodicity of the convective events.

1. Introduction

Focus of this study is the investigation of a possible link between the southern high-latitude (sub)surface conditions and the variability of water mass properties and flow along the deep western boundary of the (sub)tropical Atlantic. Though weak, there is some observational evidence for correlation between variability in Southern Ocean (SO) surface conditions, in particular, sea ice concentration, and Antarctic Bottom Water (AABW) outflow [*Comiso and Gordon*, 1998; *Fahrbach et al*., 1995; *Jacobs and Guilivi*, 1998; M. Drinkwater, personal communication, 1996]. Variability in AABW formation is most likely to occur in the high-latitude embayments of the Ross and the Weddell Seas, and respective outflow anomalies are most likely to emerge along the deep western boundaries in the southwest Pacific [*Johnson and Orsi*, 1997; *Orsi et al*., 1999] and southwest Atlantic [e.g., *Whitworth et al*., 1991; *Locarnini et al*., 1993; *Coles et al*., 1996; *Orsi et al*., 1999].

Observational evidence for possible remote effects of variations in Weddell Sea surface conditions and convection has been discussed by *Coles et al*. [1996]. On the basis of their analysis of data collected in 1988–1989 and the historical database, they suggest that deep ocean property anomalies propagate from the Weddell Sea region along the deep western boundary of the Argentine Basin up to ~18°S in the Brazil Basin in 5–11 years. Their observed temperature and salinity anomalies along isopycnals referenced at 4000 m depth in the northwestern Argentine Basin are ~0.05°C and 0.008 practical salinity unit (psu).

Further evidence for decadal variability in the flow of AABW is given by *Hogg and Zenk* [1997] on the basis of observations in the Vema Channel (at about 30°S, 40°W). This constitutes the main northward pathway for AABW from the Argentine Basin to the Brazil Basin, with a mean transport of 4 Sv [*Hogg et al*., 1999] and together with the Hunter Channel to the east and the Santos Plateau to the west ~6.9 Sv [*Hogg et al*., 1999; *Zenk and Hogg*, 1996]. *Hogg and Zenk* [1997] observed similar variability in temperature as reported by *Coles et al*. [1996], but they did not identify any changes in salinity. On the other hand, they reported variability in northward velocities in the range of ~6 cm s^{-1} and high northward velocity anomalies coinciding with cold temperature anomalies, and vice versa. Such observation has recently been confirmed by *Zenk et al*. [1999] for the Hunter Channel on the basis of additional moored current meters, which also allowed for a more detailed variability analysis.

More observed evidence for rapid and remote responses to

Paper number 2000JC000335.
0148-0227/01/2000JC000335$09.00

high-latitude surface conditions has been reported from the North Atlantic [e.g., *Curry et al*., 1998; *Dickson*, 1997; *Sy et al*., 1997; *Pickart and Smethie*, 1998; *Turrell et al*., 1999; *Molinari et al*., 1998; *Koltermann et al*., 1999].

Similar timescales of signal propagation are revealed in modeling studies which examine the response to changes in the buoyancy forcing of the Nordic seas [e.g., *Döscher et al*., 1994; *Gerdes and Köberle*, 1995; *Goodman*, 2001]. *Döscher et al*. [1994] identify the initial signal being set up by a baroclinic coastal Kelvin wave. The model phase speeds of these waves are grid-size-dependent [*McDermott*, 1996] and are typically underestimated by 1 order of magnitude in coarse-resolution models [*Goodman*, 2001]. A thorough theoretical analysis of the possible wave structure and dispersion after localized buoyancy forcing is given by *Hallberg and Rhines* [1996] based on experiments with an isopycnal model with sloping lateral boundaries.

Concerning convective instabilities, these are most likely induced by anomalous surface conditions but also by anomalous subsurface conditions. In the case of the SO this can be accomplished by anomalous inflow of North Atlantic Deep Water (NADW) or Lower Circumpolar Deep Water (LCDW) [*Whitworth et al*., 1998; *Reid*, 1996; *Comiso and Gordon*, 1998; *Jacobs and Guilivi*, 1998; *Locarnini*, 1994; *Fahrbach et al*., 1995; A. Orsi, personal communication, 1998]. Since such anomalies (provided they exist at all) would normally compensate in density, they need to interact with the surface in order to induce convective instabilities. The most likely mechanism is that promoted by, e.g., *Gordon and Huber* [1990] and *Martinson* [1990], in conjunction with the generation of an open ocean polynya, i.e., entrainment of LCDW into the winter mixed layer.

While such interactions may modify the rate of open ocean convection, the real world of present-day climate indicates the main driving mechanism for the formation of Antarctic Bottom Water being that of near-boundary convection. This mechanism involves cold and salty Shelf Water flowing down the continental slope, in the process of which it becomes mixed with the warmer and even saltier LCDW [*Whitworth et al*., 1998; *Gordon*, 1998; *Foster and Carmack*, 1976; *Gill*, 1973].

In a modeling study, *Pierce et al*. [1995] showed that warm subsurface water in the SO can lead to open ocean convective instabilities. In particular, they suggested that accumulation of LCDW triggers phases of enhanced convection. While SO sea ice is regionally rather thick (up to 15 m) in their mode of weak convection, it reduces to <0.5 m in phases of enhanced convection, leading to a reduced ice cover, which itself enhances convection due to buoyancy loss at the surface, thus leading to a positive feedback and the open ocean polynya mode [e.g., *Broecker*, 1999].

Several recent modeling studies addressed the role of high-latitude processes on long-term mean-state ocean properties and circulation. Using coupled sea ice–ocean models with seasonal climatological forcing, *Maier-Reimer* [1993], *Goosse et al*. [1997], and *Stössel* [1997] found a sensitive impact of the brine release effect on the outflow of AABW into the world's ocean and, consequently, on the global deep ocean's temperature and salinity. In a similar setting, *Stössel et al*. [1998] (hereinafter referred to as SKD) identified a series of additional such impacts arising from changes in the description of SO sea ice and its forcing from the atmosphere, the largest of which resulted from the effect of wind variability on ice growth rates. *Duffy and Caldeira* [1997], using yet another sea ice–ocean general circulation model (GCM), and *Duffy et al*. [1999], employing a sea ice–ocean GCM coupled to an energy moisture balance model, revealed significant effects of their global ocean model properties on changes in the way released brine is initially distributed in the water column. *Goosse and Fichefet* [1999] extended their earlier studies by adding a series of idealized experiments to isolate the role of ice ocean fluxes on the world ocean's circulation.

Concerning variability, most of the experiments conducted by SKD revealed a pronounced quadrennial oscillation, which was largely confined to the Weddell Sea region and involved the Drake Passage throughflow [*Stössel and Kim*, 1998]. The pronounced variability of the latter gave rise to regional subsurface temperature anomalies in the northern branch of the Weddell Gyre, which tended to disperse southward and to modify sea ice concentration in the central gyre. This imprint appeared to advect southward to finally modify convection in the extreme southern Weddell Sea, with negative ice concentration anomalies enhancing convection, and vice versa. This, in turn, induced deep ocean temperature and salinity anomalies.

While this internal sea ice–ocean oscillation was robust in most of SKD's experiments, a transition to a decadal basin-scale mode emerged when turbulent heat fluxes were enhanced to more realistic values (the magnitude of change being of the order of that associated with switching the wind vector forcing from monthly climatological to daily real-time values). Further analysis revealed that a decisive cause for the change in the mode of variability is the magnitude of heat flux over subgrid-scale leads within the SO sea ice pack. The decadal mode has similarities to the quadrennial mode described above but also has important differences, one of which being its remote effect on the outflow of NADW.

The aim of this study is to investigate the mechanism of this decadal mode, describing its northward propagation and its impact on the deep (sub)tropical Atlantic. This will be elaborated in section 3, followed by a discussion of the results, and a mechanism that may explain why the model oscillation is self-sustaining. In section 2 the model will be described.

2. The Model

Since we are interested in the variability about a long-term mean state of the deep ocean, the strategy consists of using a model which allows for a series of near-equilibrium experiments. Therefore a coarse-resolution model is employed. The criteria for a near-equilibrium solution were adopted from *England* [1993], i.e., a climate drift of global mean temperature and salinity of <0.01°C and <0.001 psu, respectively, per century for all model layers.

In particular, we use a global coarse-resolution ($3.5° \times 3.5° \times 11$ layer) version of the Hamburg Ocean Primitive Equation (HOPE) model [e.g., *Latif et al*., 1994; *Drijfhout et al*., 1996; *Wolff et al*., 1997; *Marsland and Wolff*, 1998; *Legutke and Maier-Reimer*, 1999], which includes a comprehensive sea ice model with ice dynamics based on the work by *Hibler* [1979] and ice thermodynamics based on the work in *Owens and Lemke* [1990] [SKD; *Stössel et al*., 1996; *Legutke et al*., 1997]. The z level model includes a prognostic free sea surface and a depth discretization which follows the actual bathymetry (same scheme as described by *Maier-Reimer et al*. [1993]).

The specific model configuration used in this study is that described by SKD. It is based on the version of *Drijfhout et al*.

[1996] and is driven by climatological, monthly mean winds, and temperature and salinity restoring (with winds from *Hellerman and Rosenstein* [1983], air temperature from *Woodruff et al*. [1987], restoring timescale of 80 days, and salinity from *Levitus* [1982], restoring timescale of 40 days). Further details are given by *Drijfhout et al*. [1996]. Compared to the latter, SKD introduced several upgrades to the treatment of sea ice, as summarized in the following.

In grid cells that contain sea ice, a separate, subgrid-scale calculation of the surface heat balance has been attempted to account for the extreme differences in heat flux over ice-free and ice-covered parts of a model grid cell. For the heat balance calculation over ice-free parts, the sea surface temperature is kept at the freezing point, while the heat flux over ice is determined by iteratively adjusting the ice surface temperature to the ambient conditions [*Maykut*, 1986]. No salinity restoration is applied under sea ice, assuming that there the freshwater flux is provided by the process of freezing and melting.

As mentioned in section 1, the crucial parameter for the decadal mode to sustain is an enhanced turbulent heat flux over subgrid-scale leads. This condition is associated with a globally much cooler and fresher deep ocean (see SKD) and is mainly a response to the overall enhanced AABW formation due to enhanced new ice formation in SO leads. The term "new ice" refers to ice formed at an initially ice-free surface. This constitutes a highly nonlinear process, depending sensitively on ice concentration, and is in the SO associated with the bulk of brine release. Under typical cooling conditions, new ice growth rates can be up to 10 cm d^{-1} [*Maykut and Untersteiner*, 1971; *Leppäranta*, 1993]. With a model time step of 20 hours, this is about the maximum thickness an overfrozen model lead can attain before getting redistributed in a subsequent time step.

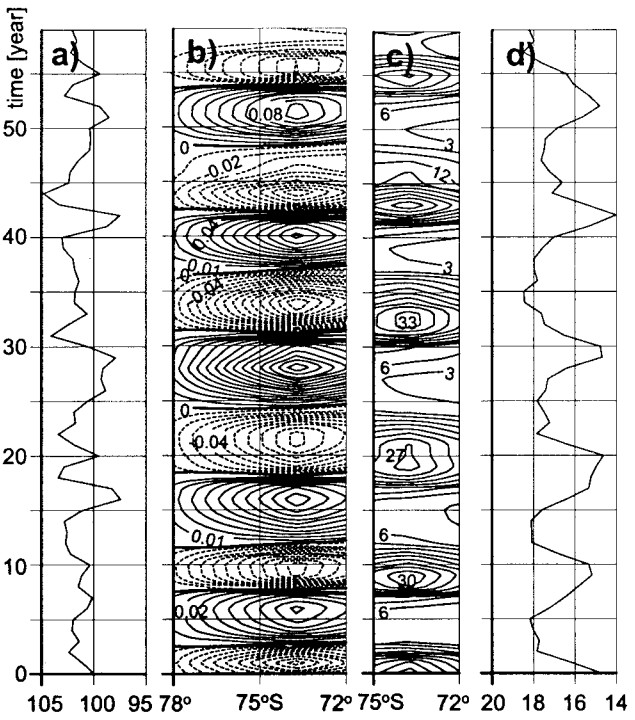

Figure 1. Sixty-year time latitude diagrams along 35°W of (c) potential energy release due to convection from 72°S to 75°S (increment 3 mW m^{-2}), (b) 3000-m temperature anomalies from 72°S to 78°S (increment 0.01°C), and time series of (d) NADW outflow across 30°S and (a) Drake Passage throughflow, both in Sv (1 Sv = 10^6 m^3 s^{-1}).

3. Description of the Results

The results are described in three phases: the character of the decadal mode, the northward propagation of AABW anomalies, and their impact on NADW outflow. All data shown are annual means, unless noted otherwise.

3.1. Mode of Variability

The most striking features sustained in this model are illustrated in Figure 1. Large variations are seen in convective potential energy release at 74°S, 35°W (Figure 1c) and, subsequently, at the same position in deep ocean temperature (Figure 1b) and salinity (not shown). These variations are ~3 times stronger than with the quadrennial mode discussed by *Stössel and Kim* [1998, Figure 3]. Furthermore, the Drake Passage throughflow (Figure 1a) does not follow the variations in convection as opposed to the quadrennial mode. Instead, the NADW outflow features strong oscillations (Figure 1d), which are highly correlated with the southern high-latitude convective events.

Furthermore, the quadrennial mode is characterized by a quasi-instantaneous (barotropic) dynamic response, whereas the stronger anomalies of the decadal mode are predominantly baroclinic in nature. This is illustrated in Figures 2 and 3 in terms of the time-space behavior of the model's mass field in the Weddell Sea. Figure 2 shows 30-year time-space diagrams of zonal sections between 60°W and 30°W of temperature anomalies averaged over the entire water column (Figure 2a) and of sea level anomalies (Figure 2b), both for the quadrennial mode. The same is shown in Figure 3 over 60 years for the decadal mode. Figures 2 and 3 represent meridional averages between 65°S and 80°S. While the temperature anomalies reveal a clear westward propagation in both cases, the sea level anomalies follow synchronously only with the decadal mode.

3.2. Northward Propagation of AABW Signals

The larger amplitudes of the decadal deep ocean temperature variations give rise to AABW anomalies which propagate along the deep western boundary, i.e., the model's Drake Passage sill (depth ~2500 m) and the model's Scotia Ridge (depth ~3500 m), thus underriding the Antarctic Circumpolar Current (ACC) (see Figure 11 for the lateral boundaries for model variables centered at 3000 and 4000 m).

A time-space diagram, in which the spatial dimension is chosen to follow the western boundary of the ninth model layer (centered at 3000 m), is shown in Figure 4 in terms of temperature anomalies for a 100-year period from 75°S, 30°W (point 1) to 10°S, 35°W (point 18). There is a slow but prominent signal propagation from point 1 to point 6 at the tip of the Antarctic Peninsula. Beyond that point, entering the ACC region, the anomalies become severely distorted. Nevertheless, it appears that the same cluster of variability emerges beyond 40°S (i.e., point 11).

A clearer indication of a correlation is given in Figure 5, where the temperature variations at 70°S, 50°W, 3000 m (solid curve) are compared with those at 30°S, 35°W, 4000 m (dashed curve) (note that the subtropical signal has been amplified by factor 5). As can be depicted from Figure 5b, the 200-year time series of both fields are highly correlated, with the polar signal leading by 3–5 years.

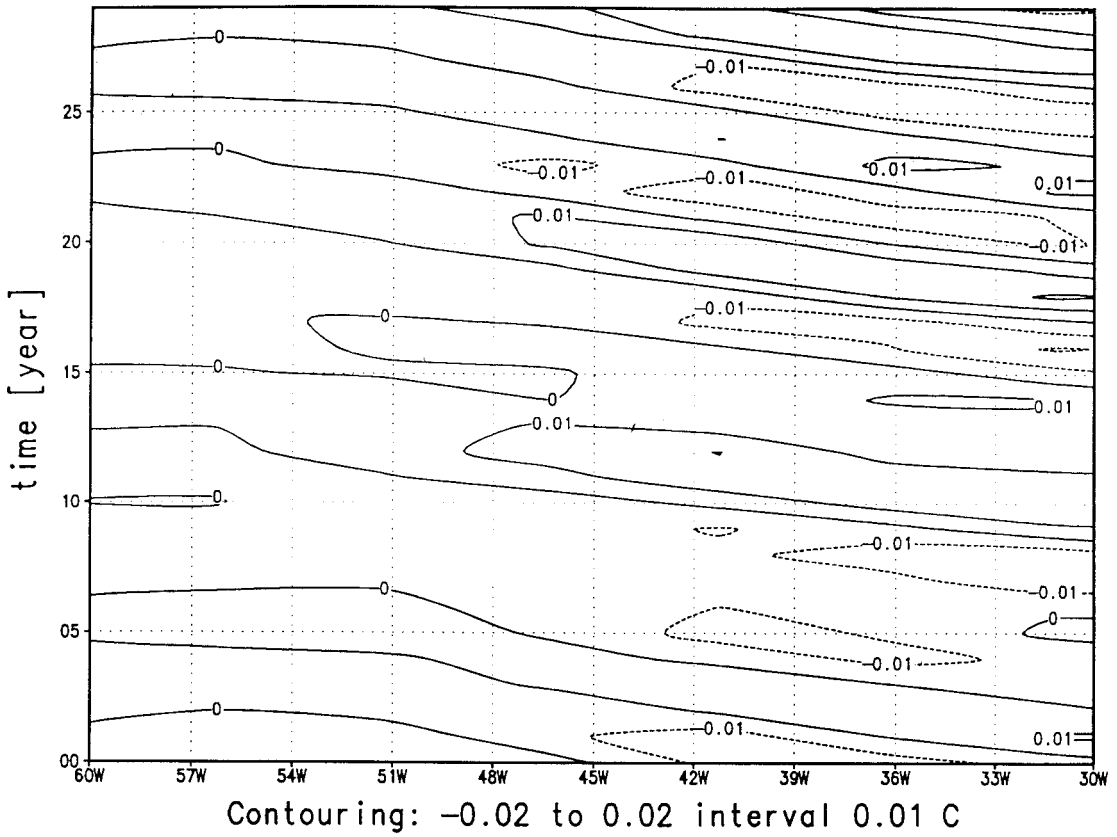

Figure 2. Thirty-year time-longitude diagram from 60°W to 30°W of (a) vertically averaged temperature anomalies and (b) sea level anomalies averaged between 65°S and 80°S for the quadrennial mode.

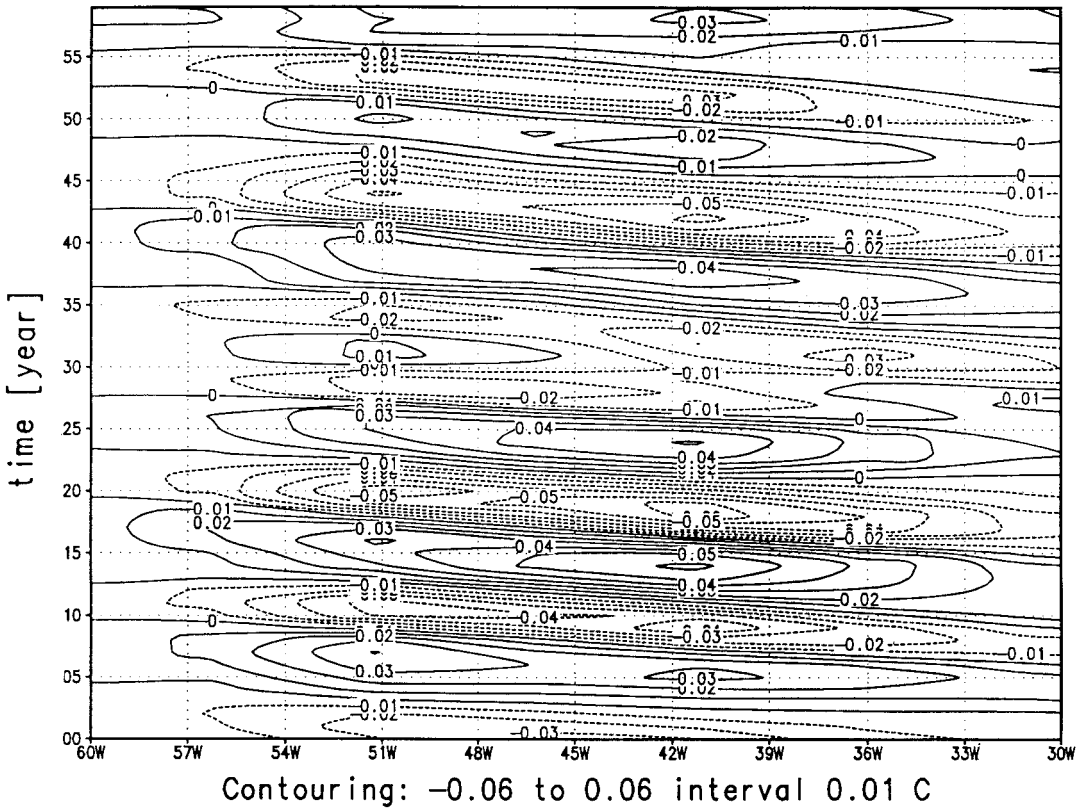

a

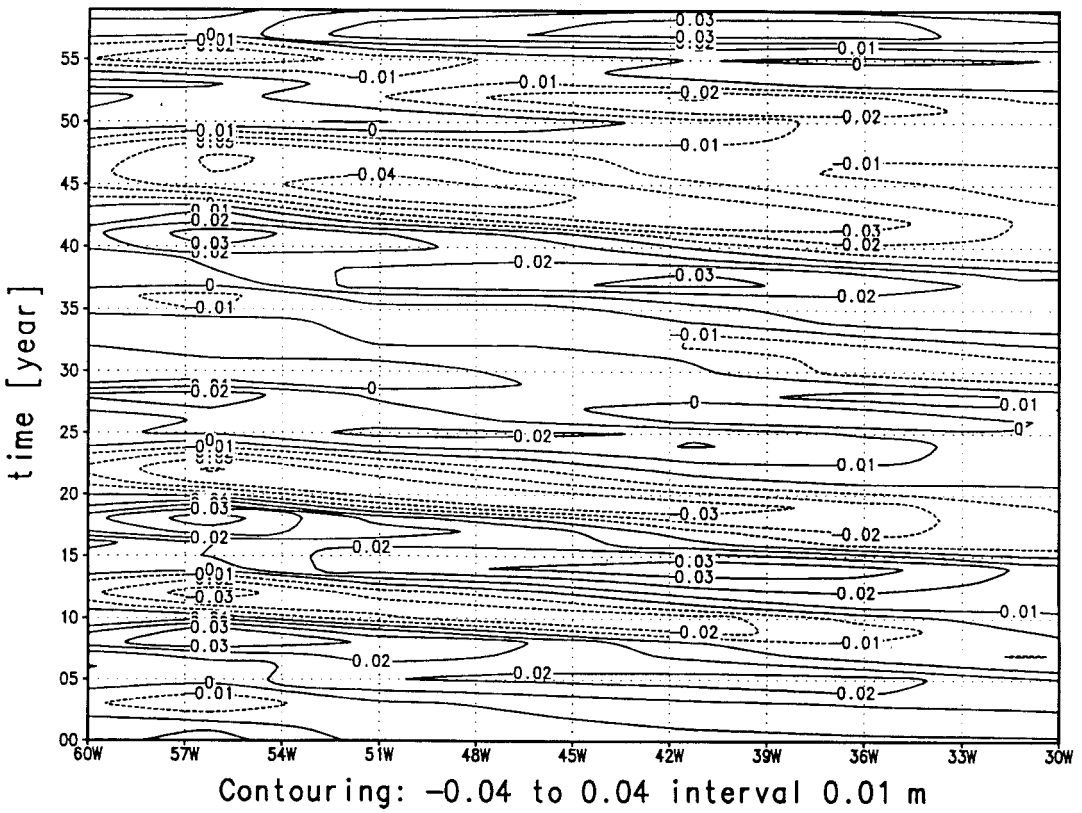

b

Figure 3. Sixty-year time-longitude diagram for the decadal mode; otherwise as Figure 2.

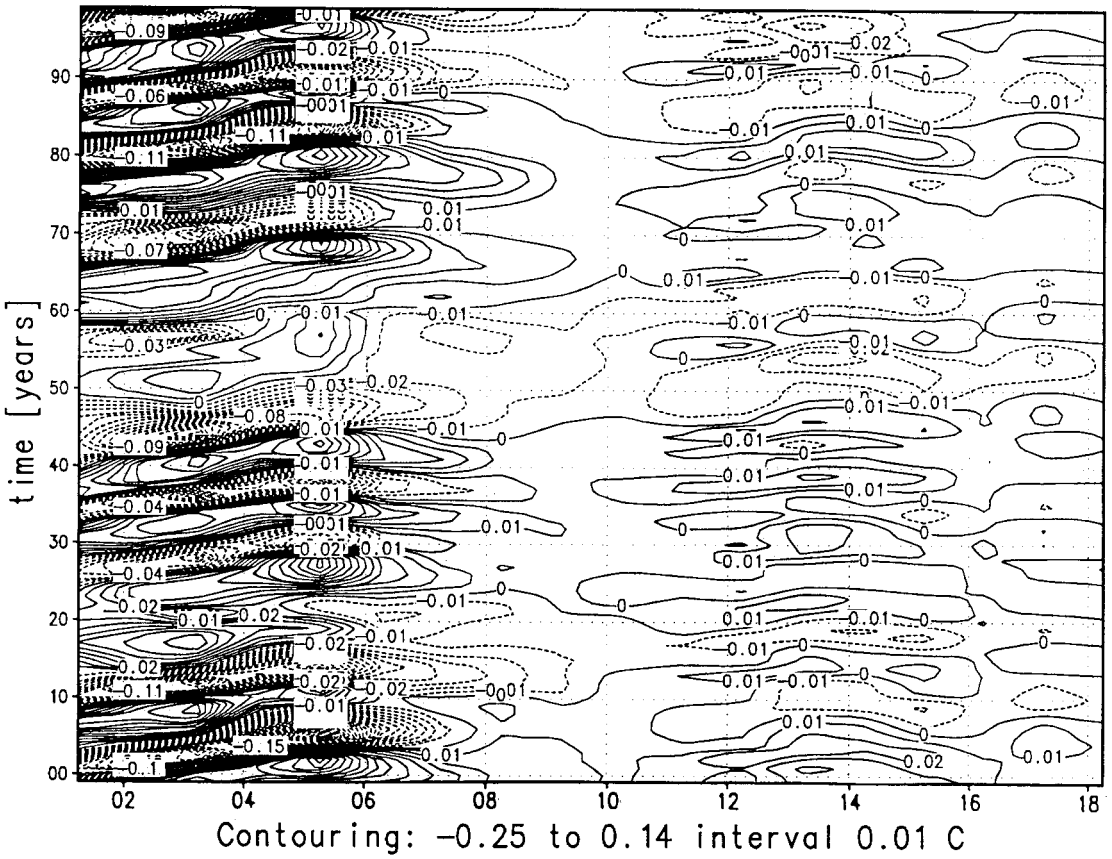

Figure 4. One-hundred-year time-space diagram of 3000-m temperature anomalies along the deep western boundary from 75°S, 30°W (point 1) to 10°S, 35°W (point 18).

This feature is further supported by lagged correlation patterns in which the sea surface elevation has been correlated with convection at 74°S, 35°W (Figure 6). Consistent with Figures 1c to 1b, maximum negative correlation with deep ocean temperature, and thus sea level at 74°S, 35°W (Figure 3), occurs after one year (lag 1). This signal propagates slowly westward. Upon meeting the westernmost longitudes of the 3000-m model bathymetry, a rapid northward propagation follows, signals of which emerge at the equator some 4 years later. From there, they propagate eastward along the equator.

The amplitudes in 4000-m subtropical temperature variability are ~0.05°C (Figure 7), while the corresponding amplitudes in salinity are ~0.007 psu (not shown). Also, phases of colder and fresher anomalies, suggestive of enhanced AABW, are associated with northward velocity anomalies, and vice versa (Figure 7, dashed curve; note that in Figure 7 the north-south convention has been reverted, i.e., negative velocity means northward, and positive means southward).

3.3. Deep Water and Bottom Water Flow in the Subtropical Atlantic

Model "NADW outflow," defined as the net southward flow of NADW excluding the return flow of AABW across 30°S, can be calculated as the negative of the net northward meridional volume transport above the interface that separates the northward flowing intermediate water from the southward flowing NADW. As depicted in Figure 8, the variability of this quantity is highly correlated with the anomalies of AABW entering the subtropics at the western boundary of the same latitude (Figure 7).

NADW outflow can also be derived from the meridional overturning stream function of the Atlantic. Figure 9 shows this quantity, indicating a maximum AABW transport of ~7 Sv and a mean NADW outflow across 30°S of ~17 Sv, both in good agreement with what has been estimated from observations [e.g., *MacDonald and Wunsch*, 1996; *Ganachaud and Wunsch*, 2000]. In order to relate the variability of the AABW "inflow" to that of NADW outflow, stream function anomalies at 30°S, separated by those associated with AABW at 3500 m and NADW at 1500 m are monitored. The resulting 200-year time series (Figure 10) reveals a clear correlation of both, with enhanced intrusion of AABW coinciding with weakened NADW outflow, and vice versa (note sign convention, positive AABW stream function anomaly means reduced AABW inflow, and positive NADW stream function anomaly means enhanced NADW outflow). Thus, in phases of enhanced AABW inflow, less NADW exits across 30°S. Furthermore, the deep signal leads the shallower signal by 1–2 years (Figure 10b). Note that the variations of the AABW inflow are ~1 order of magnitude lower than those of the NADW outflow.

4. Discussion of the Results

In this section the model results will be discussed and related to the observational evidences reported in section 1. The issues are subdivided as in section 3.

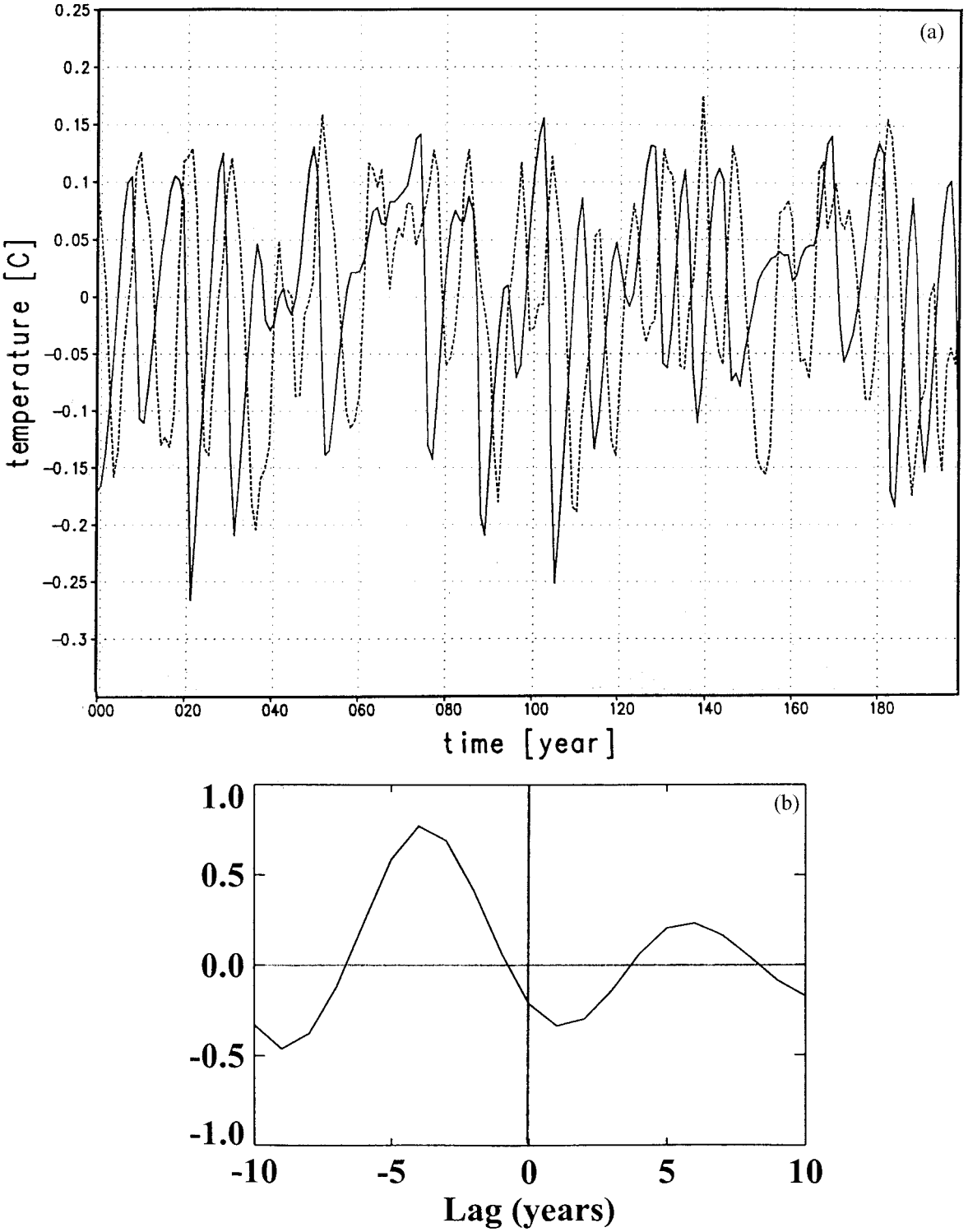

Figure 5. Two-hundred-year time series of 3000-m temperature anomalies at 70°S, 50°W (solid curve) and 4000-m temperature anomalies × 5 at 30°S, 35°W (dashed curve); (b) associated lagged correlation.

4.1. Mode of Variability

The first striking question is why the Drake Passage throughflow follows the periodic convective instabilities in the quadrennial mode, while it does not do so in the decadal mode. Following the arguments of *Hallberg and Rhines* [1996], this is probably a result of convection penetrating deeper in the latter case, inducing bottom-trapped topographic Rossby waves in deeper layers, whereas in the former case (where the anomalies are confined to shallower layers), barotropic topographic Rossby waves are excited along the boundary in the upper layers (in particular, in shallower layers than the Drake Passage sill depth). Note that a sloping or at least variable bottom topography is a prerequisite for topographic Rossby waves to exist. The latter exists in the model used here; that is, each

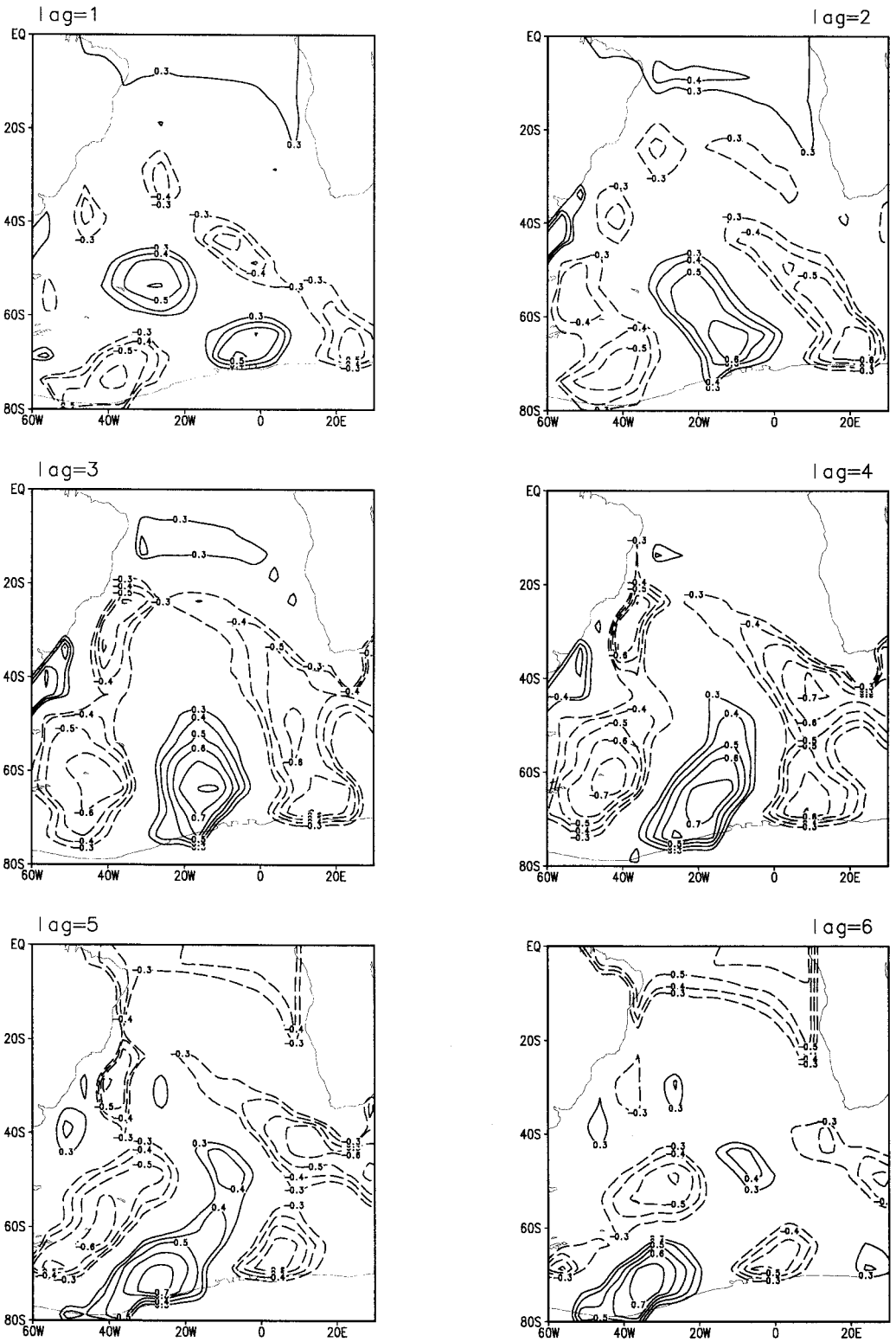

Figure 6. Correlation patterns of sea surface height against convective potential energy release at 74°S, 35°W. Lags are in years. Increment is 0.1; smallest magnitude of correlation shown is 0.3.

water column has its individual water depth following the real-world bathymetry. This could possibly allow for topographic Rossby waves to exist and provide an alternative explanation to the Kelvin wave mode typically existing in flat bottom models [*Hallberg and Rhines*, 1996; *Goodman*, 2001]. To answer this question, however, a more thorough investigation with z level models that feature variable bottom topography is needed.

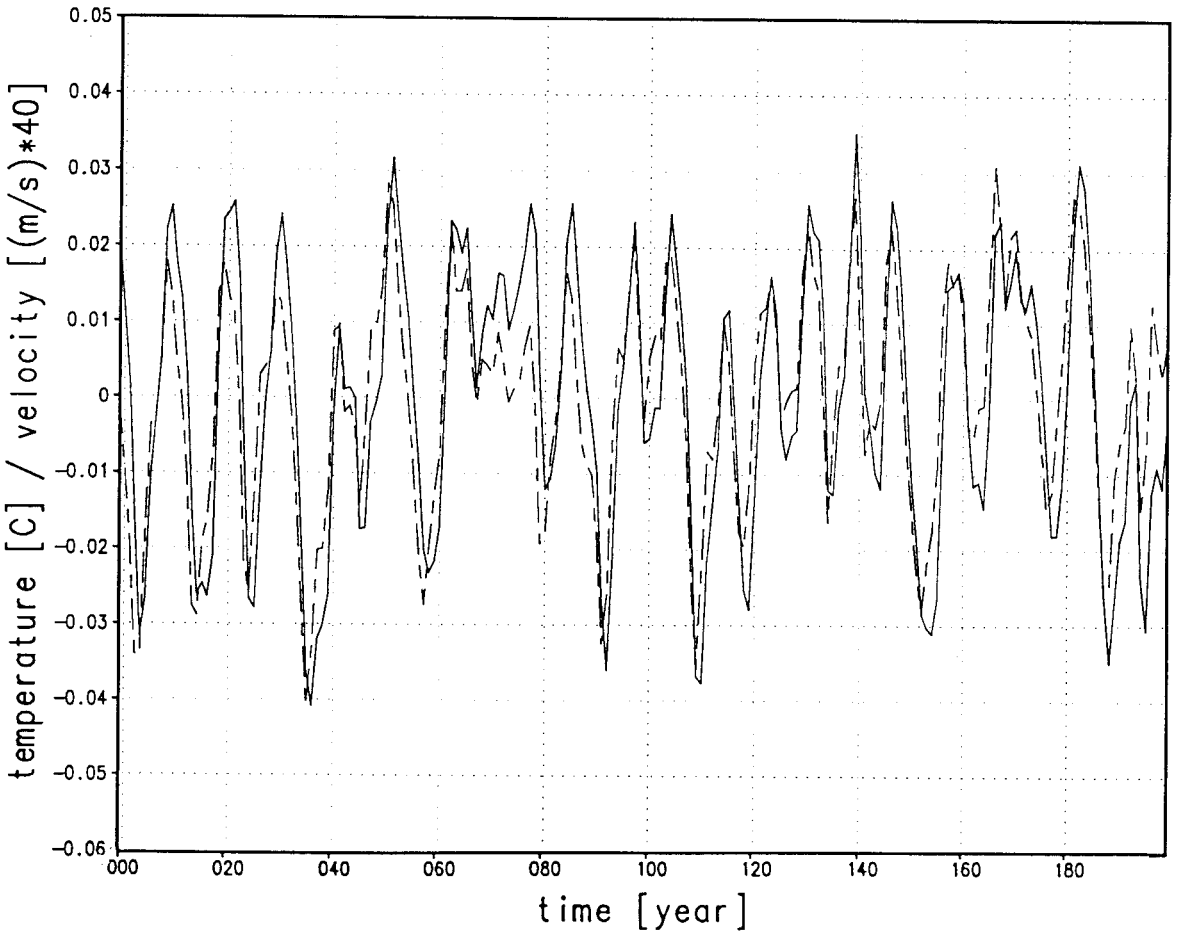

Figure 7. Two-hundred-year time series of temperature (solid curve) and southward velocity (dashed curve) anomalies at 4000 m at 30°S, 35°W. Velocities are enhanced by factor 40, i.e., $0.04 \simeq 1$ cm s^{-1}.

4.2. Northward Propagation of AABW Signals

The first question concerns the meaningfulness of the northward signal propagation. Physically, it seems plausible that periods of enhanced convection would give rise to periods of enhanced outflow of AABW into the world's ocean, and there is some observational evidence for this.

As elaborated in section 1, evidence for a more remote effect of such variability has been provided by *Coles et al.* [1996]. Their resulting travel time of anomalous water from the Weddell Sea to 18°S of 5–11 years matches the model's baroclinic adjustment timescale. This is quite striking, since the slowness of the latter is generally known to be an artifact of a model's coarse resolution. Concerning the decadal change reported by *Coles et al.* [1996], there is also remarkable agreement with the modeled amplitude of temperature and salinity changes at 4000 m depth around 30°S, 35°W. Furthermore, phases of cold anomalies coinciding with phases of northward velocity anomalies seem consistent with data reported by *Hogg and Zenk* [1997], though the associated model velocity amplitudes are 1 order of magnitude smaller. The latter is obvious, since a coarse-resolution model's boundary current cannot be as swift and confined as in nature (while the associated transport, representing an integral over a wider section, can nevertheless be correct). As a result of the agreement between phase speed of signal propagation and model AABW temperature (and salinity) amplitudes, the maximum rate of anomaly change (0.01°C y^{-1}) is also in good agreement with observations, e.g., those reported by *Hall et al.* [1997] from the abyssal equator or *Zenk and Hogg* [1996] from the Vema Channel. Since their figures are based on records of barely 2 years, the implied "trends" could just be a reflection of a longer-term (e.g., decadal) variability.

To summarize, for the given model resolution the timescale of the model's anomaly propagation along the deep western boundary is consistent with the baroclinic adjustment to perturbations in high-latitude buoyancy forcing. On the other hand, the propagation timescale as well as the water property amplitudes also agree with that retrieved from observations.

4.3. Deep Water and Bottom Water Flow in the Subtropical Atlantic

Another striking result in our simulation is the fact that southward flow of NADW across 30°S decreases with enhanced northward flow of AABW, and vice versa. Furthermore, AABW anomalies lead NADW anomalies, and the latter are 1 order of magnitude larger than the former.

The first feature is mostly a reflection of the interface between AABW and NADW going up (down) with enhanced (weakened) northward flow of AABW (Figure 9). This is similar to the observation of *Hall et al.* [1997] in the western tropical Atlantic, although they refer to the interface between AABW and lower NADW (LNADW) (the latter includes the

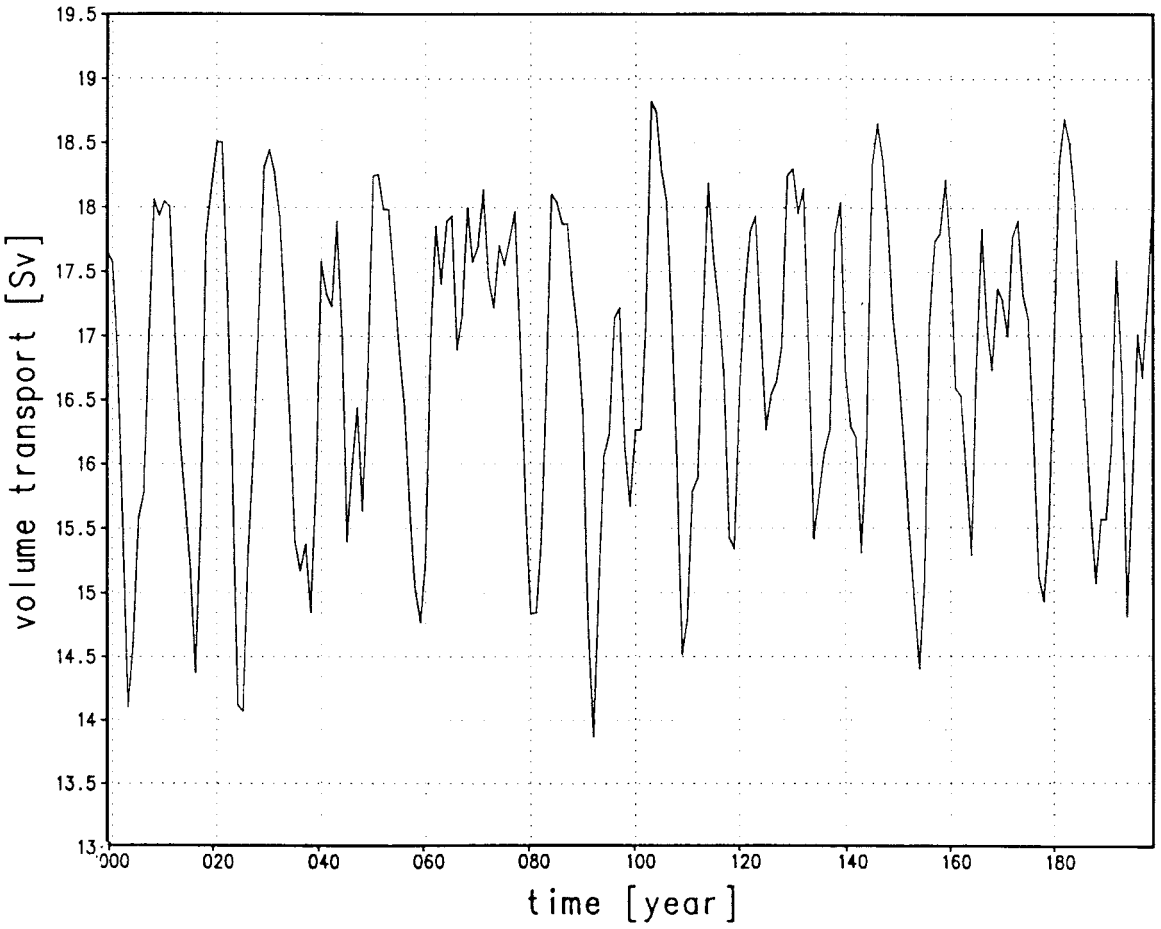

Figure 8. Two-hundred-year time series of NADW outflow across 30°S.

return flow of AABW). On the basis of a 604-day record of moored current meters, they report substantial variability in the westward flow of AABW (from the Brazil Basin to the Guiana Basin at the abyssal equatorial passage). They stress that phases of enhanced (reduced) AABW flow coincide with phases of reduced (enhanced) eastward flow of LNADW and an ascent (descent) of the transition layer between AABW and LNADW.

While this cannot be distinguished in the meridional overturning stream function of the 11-layer z level model used here, by mass conservation an enhanced AABW inflow in the lowest layer(s) would result in an enhanced AABW return flow in shallower layers. If the enhanced mass transport of the latter is mainly a result of AABW (including its return flow) occupying a larger volume, as indicated in Figure 9 by the elevated zero streamline around 3000 m, a reduced NADW outflow is the consequence, at least on short-term (i.e., the baroclinic adjustment timescale). The boundary flow anomalies are expressions of the particle motion of the boundary wave, while the vertical property displacements coincide with the amplitude of the wave. This gives rise to the short-term variability in the volume transports shown in Figures 8–10. In this discussion we assume no mixing of AABW with NADW north of 30°S, and, to ensure that the NADW outflow does not include an AABW component, we measure NADW outflow as the negative of the inflow above 1500 m, where the temporally and zonally averaged flow is always northward (see section 3.3). *Hall et al*.'s [1997] observations are comparable with our model results in that at times of stronger AABW intrusion AABW occupies a larger part of the water column, thus moving the layer of the southward (or eastward) flowing LNADW upward. This leads to a weakening of LNADW outflow at deeper layers (as shown by *Hall et al*. [1997] but not distinguished in our model), and a weakened outflow of "genuine" NADW (as shown in our model, but not discussed by *Hall et al*. [1997]).

Another correspondence with *Hall et al*.'s [1997] observation is a trend in AABW transport of 0.2 Sv over a period of ~250 days. The order of magnitude of this rate of change is in line with that of the model's decadal change of AABW transport (Figure 10a).

The magnitude of variability of the southward NADW transport being ~10 times larger than that of the northward AABW transport seems to be related to the fact that NADW does not feature a well-defined boundary current beyond 20°S [*Müller et al*., 1998; *Zangenberg and Siedler*, 1998]. In particular, *Zangenberg and Siedler* [1998] observe a reduction from 22 to 6 Sv between 19°S and 30°S and explain an eastward and northeastward branching of two thirds of the flow by potential vorticity constraints due to the regional bathymetry. The eastward branching at those latitudes have also been observed by *Hogg et al*. [1999] and modeled by *Stramma and England* [1999]. Concerning this eastward branching, our results actually compare quite well with those of Stramma and England's "fine resolution model" (Figure 11 versus their Figure 9b). A large part of the NADW volume transport may thus go along rather than across 30°S, rendering the actual NADW outflow rather

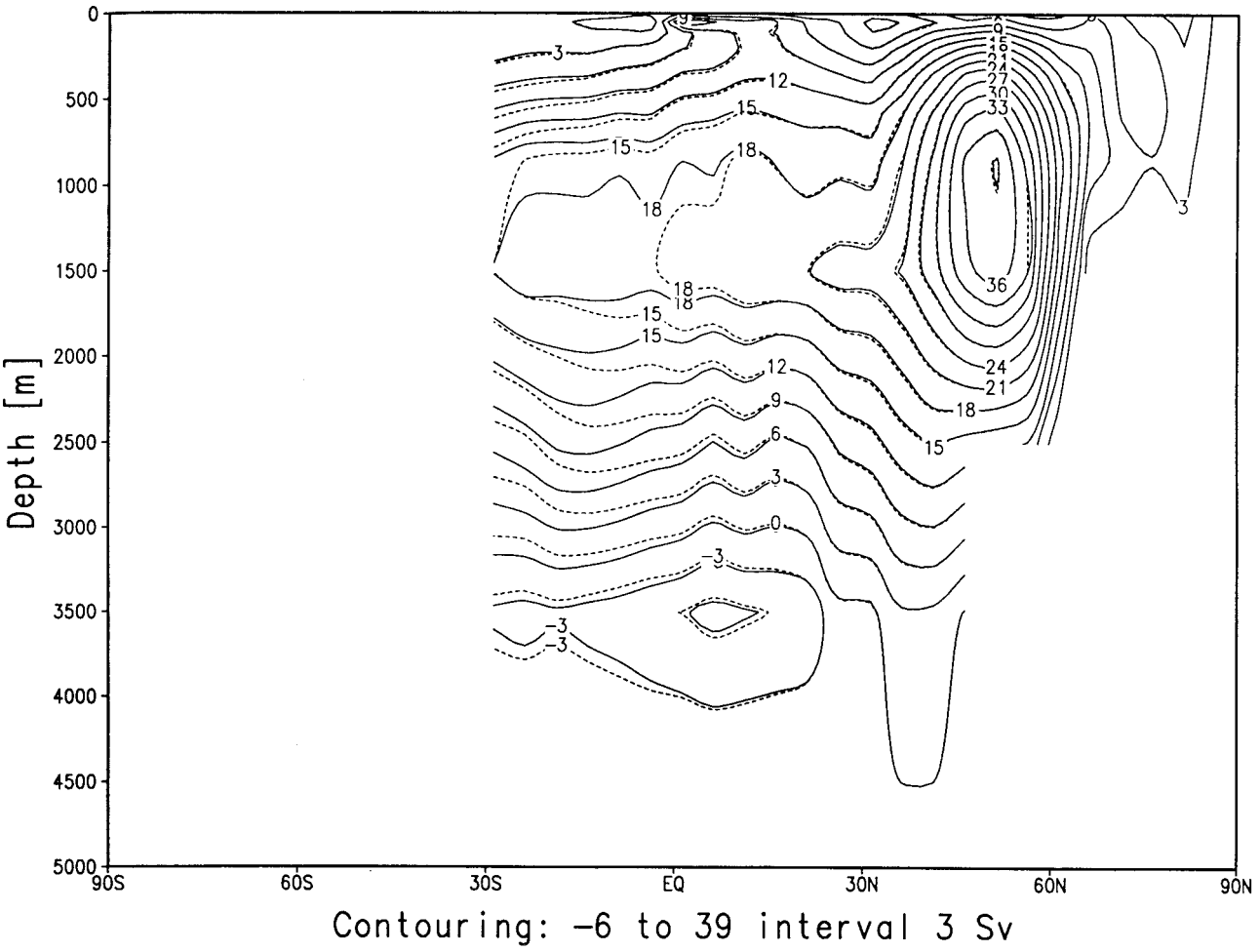

Figure 9. Atlantic meridional overturning stream function. Difference between solid and dashed streamlines indicates typical range of model variability over one decade.

susceptible to short-term fluctuations. Consistent with this explanation is the fact that the amplitude of the variability reduces rapidly northward from 30°S (Figure 9). Rather than being reduced (enhanced), the flow of NADW gets periodically diverted eastward (southward), thus periodically contributing less (more) to the actual NADW outflow. This has not been observed but is also not expected to be distinguishable with the current methods of estimating transports across sections. In fact, the 3–5 Sv NADW outflow variability (Figure 8) is within the error margins of and discrepancies between the most recent estimates from observational data with inverse methods [e.g., *Ganachaud and Wunsch*, 2000; *Sloyan and Rintoul*, 2001]. Note again that we defined NADW outflow to not include the AABW return flow.

Anomalies in NADW outflow could in principle also result from anomalies at its source region (see section 1). However, such do not occur in our model. The NADW outflow anomalies are thus unambigiously related to the AABW inflow anomalies, as can be inferred from Figure 10b.

4.4. Mechanism for Self-Sustaining Variability

Another main feature of this simulation is the self-sustained character of the oscillation. The following hypothesis is supported by the present results. The correlation patterns of the sea level anomalies associated with the periodic convective events in the southern Weddell Sea shown in Figure 6 indicate the propagation of baroclinic Kelvin waves westward and northward along the deep western boundary and eastward along the equator. The correlation patterns do also reveal the advective path of the model's Weddell Gyre. This is indicated at lags 4–6, when the negative patch at about 50°S and 40°W bulges out from the main anomaly and propagates gradually eastward with the average speed of the model's ACC. The decadal model oscillation being fairly symmetric, lag 6 is quasi-opposite in phase to lag 1. Thus, following the propagation with opposite sign from there, the signal can be traced to proceed eastward and gradually southward, joining an anomaly that has propagated from the east (presumably as a baroclinic boundary wave along Antarctica). Both signals merge and reinforce at the critical convection site to finally close the decadal loop with the approximate path and timescale of the model's Weddell Gyre. Figure 11 sketches the main mechanisms believed to be involved with the model variability. The thin line indicates the path of Kelvin wave propagation with the model's baroclinic adjustment timescale, while the thick line illustrates the regional path of anomaly propagation with the advective timescale.

The temperature and salinity changes that precondition the convective instabilities are mainly confined to the upper 1000 m. The preconditioning seems to occur through LCDW

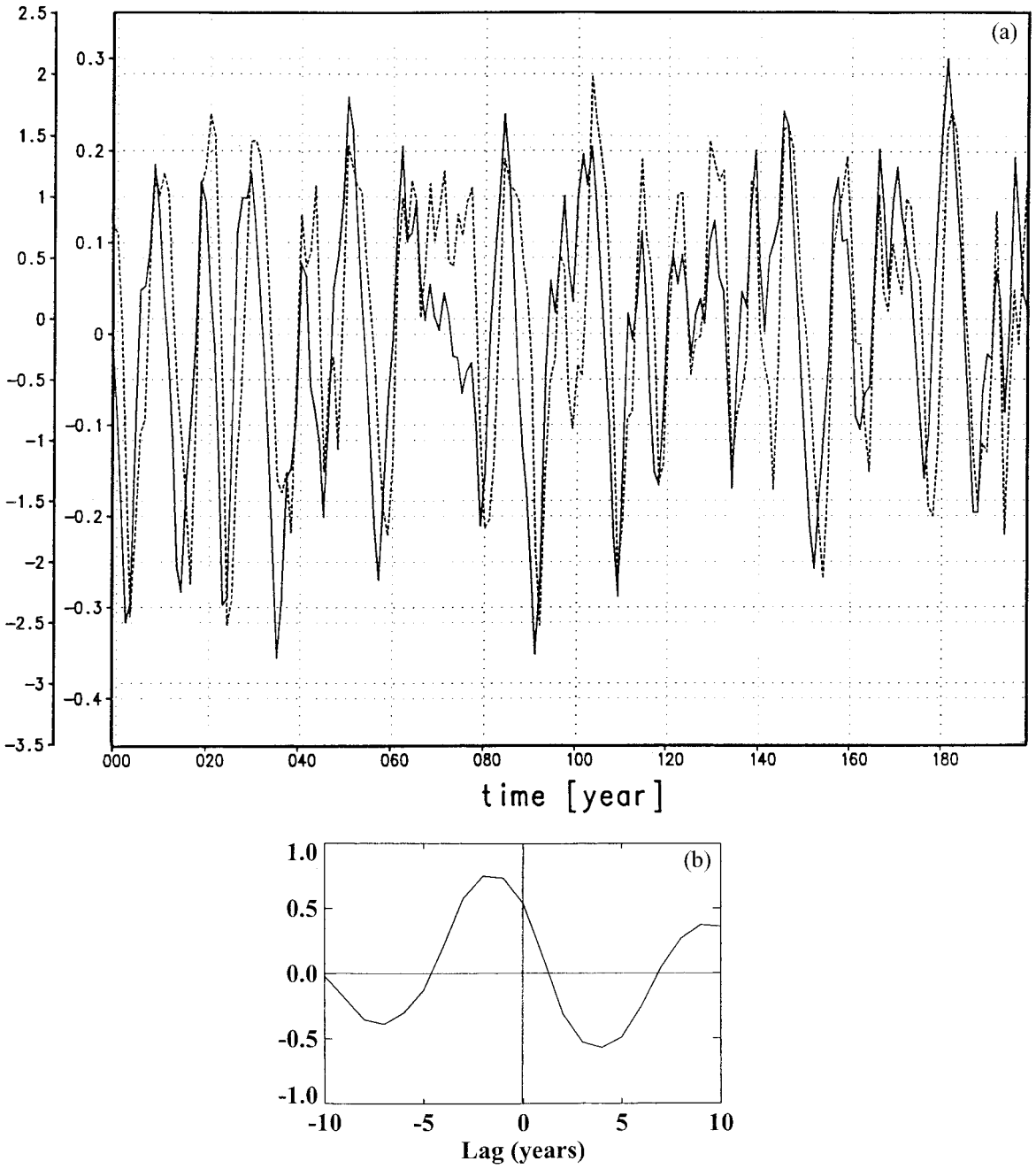

Figure 10. (a) Two-hundred-year Atlantic overturning stream function anomalies at 30°S at 3500 m (solid curve; right ordinate) and at 1500 m (dashed curve; left ordinate; units in Sv); (b) associated lagged correlation.

anomalies penetrating to the critical high-latitude Weddell Sea region. In particular, the results suggest that entrainment of warm and salty LCDW anomalies create anomalously warm and salty mixed-layer properties, which, as a result of increased surface heat loss, favor regional convective instabilities.

In this conjunction, there are two interesting questions to discuss: what role does sea ice play in this mechanism, and what are the causes for the LCDW anomalies? Figure 12 shows a strong anticorrelation between sea ice thickness and convection at the critical high-latitude convection site; that is, phases of low ice thickness are correlated with high convection, and vice versa. As with a warmer mixed layer enhancing surface cooling, and thus buoyancy loss, thinner ice has a similar effect in that ice formation and thus brine release are enhanced. Both tend to destabilize the water column. Once deep convective overturning sets in, more warm water is brought to the surface, and the feedback is positive.

Concerning the possible causes for LCDW anomalies in the Weddell Sea other than anomaly advection with the Weddell Gyre, one could be tempted to link them to NADW outflow anomalies (e.g., such as excited in our model). From the observed flow field, one could actually expect LCDW anomalies resulting from hypothetic NADW outflow anomalies to enter the eastern portion of the Weddell Gyre [*Orsi et al*., 1993], and

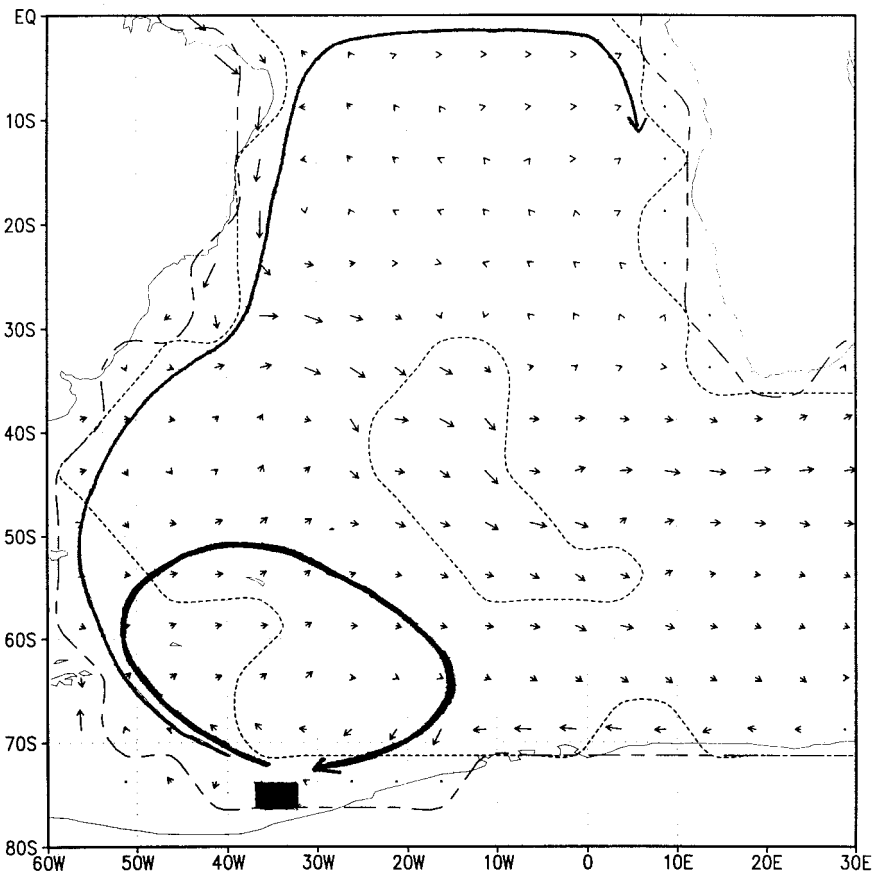

Figure 11. Model boundaries for variables at 3000 m (long-dashed lines) and 4000 m (short-dashed lines). Arrows indicate ocean currents at 2000 m depth; maximum arrow is 2 cm s^{-1} (only every other model vector is plotted). A sketch of the critical convection site around 74°S, 35°W is superimposed, as well as the path of Kelvin wave propagation associated with the baroclinic adjustment (thin line) and of anomaly advection (thick line).

via that path possibly modify convection in the southern part of the Weddell Sea. This is also supported by *Reid* [1996, p. 37], who interprets the distinct observed salinity maximum in the Weddell Sea as a reflection of a "return flow of some of the more saline water that has joined the Weddell Sea gyre and turned southward and westward along the coast of Antarctica." LCDW being characterized by a pronounced salinity maximum that clearly links it to NADW [e.g., *Whitworth et al*., 1998], even though it has traveled at least once around Antarctica, suggests that anomalies in NADW outflow could emerge as anomalous LCDW in the Weddell Sea.

Some issues discussed in this section can be compared to the findings of *Pierce et al*. [1995] (see section 1). They also report about periodic convective events in the SO that are initiated by elevated subsurface temperatures. In the language of this paper, they argue that this occurs because of LCDW accumulation up to the point when the water column becomes unstable. Besides employing a simpler sea ice–ocean GCM and different surface boundary conditions, the timescale of their oscillations between periods of enhanced and reduced SO convection is of the order of 300 years, i.e., much longer than our decadal oscillations, suggesting that different mechanisms are at play. In particular, *Pierce et al*.'s [1995] oscillations involve changes in the overall thermohaline circulation, promoting a mechanism on the global advective timescale, which does definitely not occur in our case.

5. Summary and Conclusions

In this paper we described a decadal, basin-scale mode of variability that was excited in a global sea ice–ocean GCM simulation. The surface forcing of the model is monthly and has an annual repeat cycle. The decadal mode of variability involves periodic events of enhanced convection in the southern high latitudes, amplitudes of which are most pronounced in the southern Weddell Sea. This leads to deep ocean temperature (and salinity) anomalies propagating northward along the deep western boundary to the tropical Atlantic, matching the timescale of the model's baroclinic adjustment. These anomalies modify the outflow of NADW in the sense that stronger AABW intrusion leads to weaker NADW outflow, and vice versa. The thus induced NADW anomalies propagate southeastward joining the ACC and thus contributing to LCDW. On the other hand, anomalies resulting from the periodic convective events in the southern Weddell Sea tend to advect with the Weddell Gyre, the timescale of a full cycle of which matches that of the decadal oscillation. In any case, entrainment of anomalous LCDW into the winter mixed layer seem to provide the preconditioning for periodic convective instabilities.

While the underlying dynamics and timescales of the described variability are consistent within the model environment, it is quite challenging to compare them to the real world.

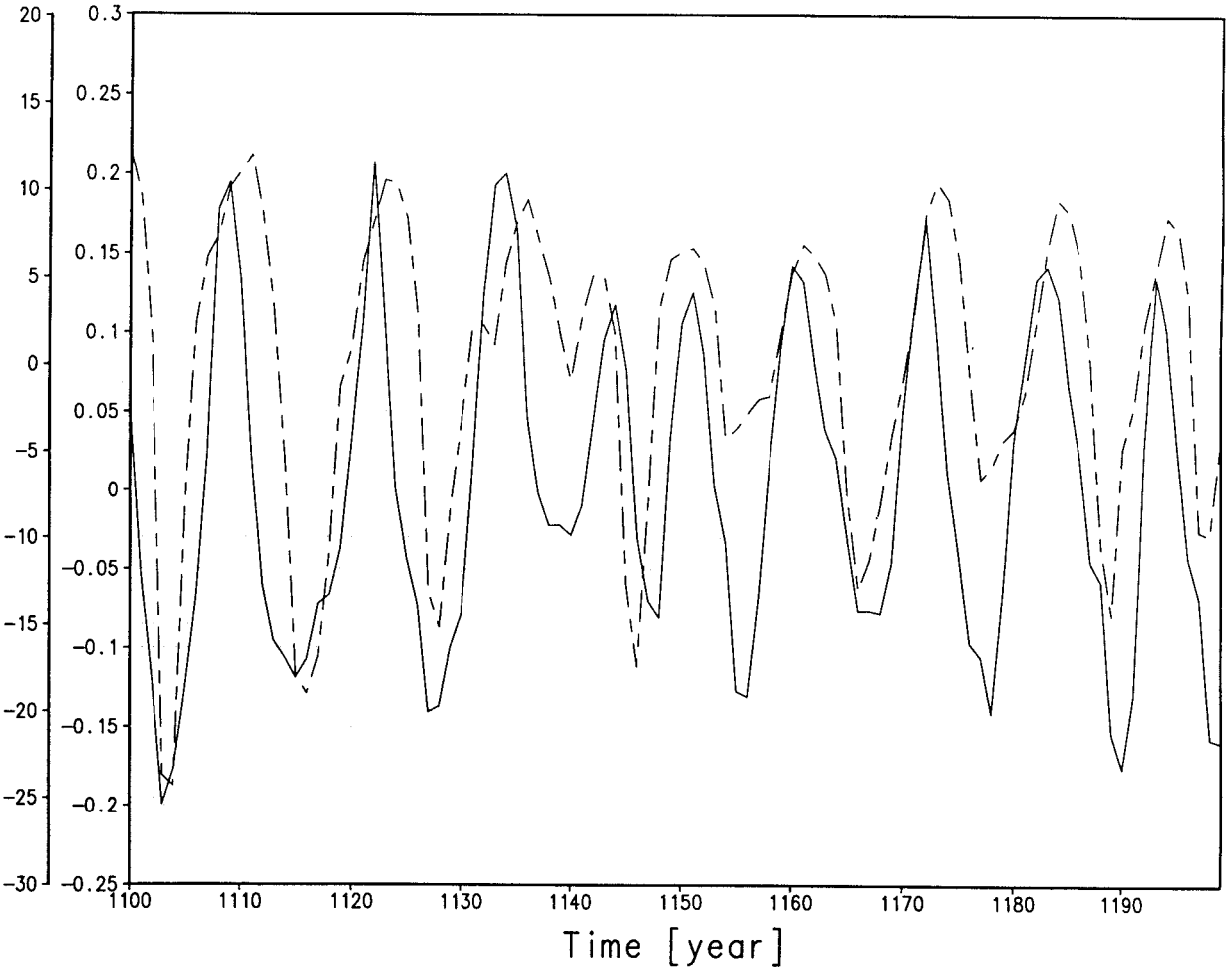

Figure 12. One-hundred-year time series of anomalies of ice thickness (solid curve; right ordinate; units in m), and negative convection (i.e., times −1; left ordinate; units in mW m^{-2}) at 74°S, 35°W (dashed curve).

There is nevertheless strikingly close resemblance of some of the modeled features to what has so far been observed. This is in particular true for the timing and the amplitude of variability and trends in AABW along the deep western boundary of the South Atlantic, similar features being observed along the North Atlantic's deep western boundary in association with perturbations in the formation of NADW, in particular Labrador Sea Water.

The peculiar and, from the modeling viewpoint, challenging aspect of the southern high latitudes is the fact that surface conditions in areas of weak stratification are nonlinearly interacting with sea ice processes. An important prerequisite for a meaningful study using an ocean GCM (OGCM) is thus the inclusion of a comprehensive dynamic-thermodynamic sea ice component, as is done here. As evident from this study, the way subgrid-scale leads, for example, are treated can become crucial.

Besides an interactive sea ice component there are a series of other factors to be considered in future studies. Among others, this study suffers from relative coarse model resolution, from not being coupled to an atmosphere model, and from a crude convection parameterization. Concerning the latter, the employment of a more detailed subgrid-scale plume convection scheme [*Paluszkiewicz and Romea*, 1997] in our model yields a much more realistic simulation of regional high-latitude processes as well as global deep ocean properties [*Kim and Stössel*, 2001].

A more realistic feedback with the atmosphere [e.g., *Rahmstorf and England*, 1997] would presumably reduce the heat fluxes over anomalous sea ice, though it is not evident how this works over subgrid-scale heterogeneities, as occur over a sea ice–ocean admixture. Ultimately, the atmospheric feedback problem will be solved by a coupling of the sea ice–ocean surface to an atmosphere model which includes detailed boundary layer physics that can handle subgrid-scale surface inhomogeneities in a physically consistent manner.

Concerning the coarseness of the model, this seems to primarily affect the formation process of AABW by not adequately simulating the accumulation of shelf water and the mixing processes with CDW along the slope [*Gordon*, 1998]. This problem has been addressed by *Kim and Stössel* [1998]. Additional experiments confirm that unrealistic deep shelf topography at the critical convection site in the model's Weddell Sea contribute to sustaining the oscillation presented here. In addition, monthly mean climatological wind forcing and the convective adjustment parameterization contribute to supporting the decadal mode in otherwise the same model configuration.

Thus the existence of the described oscillation seems to depend on a subtle combination of several southern high-

latitude sea ice–ocean processes. Similar variability being observed under present-day climate conditions suggests that it may also just exist because of the current balance of interactive processes in the high-latitude SO, which is actually quite sensitive to small changes in the ambient conditions, as, e.g., small changes in the wind and freshwater flux forcing or, presumably, the intrusion of LCDW anomalies to potential AABW formation sites. Further investigation is in progress to identify what exactly triggers the oscillation in the model.

Acknowledgments. This paper benefitted from discussions with, among others, Ping Chang, Thierry Fichefet, Moritz Flügel, Rüdiger Gerdes, Hugues Goosse, Robert Hallberg, Stephanie Legutke, Thomas Whitworth, and Michael Winton. Special thanks are due to Alejandro Orsi and Sybren Drijfhout for their critical comments on earlier drafts of this paper, as well as Robert Toggweiler and four anonymous reviewers for their constructive criticism. This research was financially supported from grants provided by the College of Geosciences at Texas A&M University, as well as NASA grant NAG5-7751.

References

Broecker, W. S., A possible 20th-century slowdown of Southern Ocean deep water formation, *Science*, *286*, 1132–1135, 1999.

Coles, V. J., M. S. McCartney, D. B. Olson, and W. M. Smethie, Chain Antarctic bottom water properties in the western South Atlantic in the late 1980s, *J. Geophys. Res.*, *101*, 8957–8970, 1996.

Comiso, J. C., and A. L. Gordon, Interannual variability in summer sea ice minimum, coastal polynyas and bottom water formation in the Weddell Sea, in *Antarctic Sea Ice: Physical Processes, Interactions and Variability*, *Antarct. Res. Ser.*, vol. 74, edited by M. O. Jeffries, pp. 293–315, AGU, Washington, D. C., 1998.

Curry, R. G., M. S. McCartney, and T. M. Joyce, Oceanic transport of subpolar climate signals to mid-depth subtropical waters, *Nature*, *391*, 575–577, 1998.

Dickson, B., From the Labrador Sea to global change, *Nature*, *386*, 649–650, 1997.

Döscher, R., C. W. Böning, and P. Herrmann, Response of the circulation and heat transport in the North Atlantic to changes in thermohaline forcing in northern latitudes: A model study, *J. Phys. Oceanogr.*, *24*, 2306–2320, 1994.

Drijfhout, S. S., C. Heinze, M. Latif, and E. Maier-Reimer, Mean circulation and internal variability in an ocean primitive equation model, *J. Phys. Oceanogr.*, *26*, 559–580, 1996.

Duffy, P. B., and K. Caldeira, Sensitivity of simulated salinity in a three-dimensional ocean model to upper ocean transport of salt from sea-ice formation, *Geophys. Res. Lett.*, *24*, 1323–1326, 1997.

Duffy, P. B., M. Eby, and A. J. Weaver, Effects of salt rejected during formation of sea ice on results of a global ocean-atmosphere-sea ice climate model, *Geophys. Res. Lett.*, *26*, 1739–1742, 1999.

England, M. H., Representing the global-scale water masses in ocean general circulation models, *J. Phys. Oceanogr.*, *23*, 1523–1552, 1993.

Fahrbach, E., G. Rohardt, N. Scheele, M. Schroeder, V. Strass, and A. Wisotzki, Formation and discharge of deep and bottom water in the Northwestern Weddell Sea, *J. Mar. Res.*, *53*, 515–538, 1995.

Foster, T. D., and E. C. Carmack, Frontal zone mixing and Antarctic bottom-water formation in the southern Weddell Sea, *Deep Sea Res.*, *23*, 301–317, 1976.

Ganachaud, A., and C. Wunsch, Improved estimates of global ocean circulation, heat transport and mixing from hydrographic data, *Nature*, *408*, 453–456, 2000.

Gerdes, R., and C. Koeberle, On the influence of DSOW in a numerical model of the North Atlantic general circulation, *J. Phys. Oceanogr.*, *25*, 2624–2642, 1995.

Gill, A. E., Circulation and bottom-water production in the Weddell Sea, *Deep Sea Res.*, *20*, 111–140, 1973.

Goodman, P. J., Thermohaline adjustment and advection in an OGCM, *J. Phys. Oceanogr.*, *31*, 1477–1497, 2001.

Goosse, H., and T. Fichefet, Importance of ice-ocean interactions for the global ocean circulation: A model study, *J. Geophys. Res.*, *104*, 23,337–23,355, 1999.

Goosse, H., J. M. Campin, T. Fichefet, and E. Deleersnijder, Impact of sea-ice formation on the properties of Antarctic bottom water, *Ann. Glaciol.*, *25*, 276–281, 1997.

Gordon, A. L., Western Weddell Sea thermohaline stratification, in *Ocean, Ice, and Atmosphere: Interactions at the Antarctic Continental Margin*, *Antarct. Res. Ser.*, vol. 75, edited by S. S. Jacobs and R. F. Weiss, pp. 215–240, AGU, Washington, D. C., 1998.

Gordon, A. L., and B. A. Huber, Southern Ocean winter mixed layer, *J. Geophys. Res.*, *95*, 11,655–11,672, 1990.

Hall, M. M., M. McCartney, and J. A. Whitehead, Antarctic bottom water flux in the equatorial western Atlantic, *J. Phys. Oceanogr.*, *27*, 1903–1926, 1997.

Hallberg, R., and P. Rhines, Buoyancy-driven circulation in an ocean basin with isopycnals intersecting the sloping boundary, *J. Phys. Oceanogr.*, *26*, 913–940, 1996.

Hellerman, S., and M. Rosenstein, Normal monthly wind stress over the world ocean with error estimates, *J. Phys. Oceanogr.*, *13*, 1093–1104, 1983.

Hibler, W. D., III, A dynamic thermodynamic sea ice model, *J. Phys. Oceanogr.*, *9*, 815–846, 1979.

Hogg, N. G., and W. Zenk, Long-period changes in the bottom water flowing through Vema Channel, *J. Geophys. Res.*, *102*, 15,639–15,646, 1997.

Hogg, N. G., G. Siedler, and W. Zenk, Circulation and variability at the southern boundary of the Brazil Basin, *J. Phys. Oceanogr.*, *29*, 145–157, 1999.

Jacobs, S. S., and C. F. Giulivi, Interannual ocean and sea ice variability in the Ross Sea, in *Ocean, Ice, and Atmosphere: Interactions at the Antarctic Continental Margin*, *Antarct. Res. Ser.*, vol. 75, edited by S. S. Jacobs and R. F. Weiss, pp. 135–150, AGU, Washington, D. C., 1998.

Johnson, G. C., and A. H. Orsi, Southwest Pacific ocean water-mass changes between 1968/69 and 1990/91, *J. Clim.*, *10*(2), 306–316, 1997.

Kim, S.-J., and A. Stössel, On the representation of the Southern Ocean water masses in an ocean climate model, *J. Geophys. Res.*, *103*, 24,891–24,906, 1998.

Kim, S.-J., and A. Stössel, Impact of subgrid-scale convection on global thermohaline properties and circulation, *J. Phys. Oceanogr.*, *31*, 656–674, 2001.

Koltermann, K. P., A. V. Sokov, V. P. Tereschenkov, S. A. Dobroliubov, K. Lorbacher, and A. Sy, Decadal changes in the thermohaline circulation of the North Atlantic, *Deep Sea Res.*, *Ser. II*, *46*, 109–138, 1999.

Latif, M., T. Stockdale, J.-O. Wolff, G. Burgers, E. Maier-Reimer, M. M. Junge, K. Arpe, and L. Bengtsson, Climatology and variability in the ECHO coupled GCM, *Tellus*, *Ser. A*, *46*, 351–366, 1994.

Legutke, S., and E. Maier-Reimer, Climatology of the HOPE-G global ocean general circulation model, *Tech. Rep. 21*, German Clim. Comput. Cent., Hamburg, Germany, 1999.

Legutke, S., E. Maier-Reimer, A. Stössel, and A. Hellbach, Ocean-sea ice coupling in a global general ocean circulation model, *Ann. Glaciol.*, *25*, 116–120, 1997.

Leppäranta, M., A review of analytical models of sea-ice growth, *Atmos. Ocean*, *31*(1), 123–138, 1993.

Levitus, S., Climatological atlas of the world ocean, *NOAA Prof. Pap. 13*, 173 pp., 1982.

Locarnini, R. A., Water mass and circulation in the Ross gyre and environs, dissertation, Tex. A&M Univ., College Station, 1994.

Locarnini, R. A., T. Whitworth, and W. D. Nowlin, The importance of the Scotia Sea on the outflow of Weddell Sea Deep Water, *J. Mar. Res.*, *51*, 135–153, 1993.

Macdonald, A. M., and C. Wunsch, An estimate of global ocean circulation and heat fluxes, *Nature*, *382*, 436–439, 1996.

Maier-Reimer, E., The driving force of brine rejection on the deep water formation in the Hamburg LSG OGCM, in *Ice in the Climate System*, *NATO ASI Ser.*, *Ser. I*, vol. 12, edited by W. R. Peltier, pp. 211–216, Springer-Verlag, New York, 1993.

Maier-Reimer, E., U. Mikolajewicz, and K. Hasselmann, Mean circulation of the Hamburg LSG OGCM and its sensitivity to the thermohaline surface forcing, *J. Phys. Oceanogr.*, *23*, 731–757, 1993.

Marsland, S., and J.-O. Wolff, East Antarctic seasonal sea-ice and ocean stability: A model study, *Ann. Glaciol.*, *27*, 477–482, 1998.

Martinson, D. G., Evolution of the Southern Ocean winter mixed layer and sea ice: Open ocean deepwater formation and ventilation, *J. Geophys. Res.*, *95*, 11,641–11,654, 1990.

Maykut, G. A., The surface heat and mass balance, in *The Geophysics*

of Sea Ice, *NATO ASI Ser*., *Ser. B*, vol. 146, edited by N. Untersteiner, pp. 395–464, Plenum, New York, 1986.

Maykut, G. A., and N. Untersteiner, Some results from a time dependent, thermodynamic model of sea ice, *J. Geophys. Res*., *76*, 1550–1575, 1971.

McDermott, D. A., The regulation of northern overturning by Southern Hemisphere winds, *J. Phys. Oceanogr*., *26*, 1234–1255, 1996.

Molinari, R. L., R. A. Fine, W. D. Wilson, R. G. Curry, J. Abell, and M. S. McCartney, The arrival of recently formed Labrador Sea water in the deep western boundary current at 26.5°N, *Geophys. Res. Lett*., *25*, 2249–2252, 1998.

Müller, T. J., Y. Ikeda, N. Zangenberg, and L. V. Nonato, Direct measurements of western boundary currents off Brazil between 20°S and 28°S, *J. Geophys. Res*., *103*, 5429–5437, 1998.

Orsi, A. H., W. D. Nowlin, and T. Whitworth, On the circulation and stratification of the Weddell Gyre, *Deep Sea Res*., *40*, 169–203, 1993.

Orsi, A. H., G. C. Johnson, and J. L. Bullister, Circulation, mixing, and production of Antarctic Bottom Water, *Prog. Oceanogr*., *43*, 55–109, 1999.

Owens, W. B., and P. Lemke, Sensitivity studies with a sea ice–mixed layer–pycnocline model in the Weddell Sea, *J. Geophys. Res*., *95*, 9527–9538, 1990.

Paluszkiewicz, T., and R. D. Romea, A one-dimensional plume model for the parameterisation of oceanic deep convection, *Dyn. Ocean Atmos*., *26*(1), 95–130, 1997.

Pickart, R. S., and W. M. Smethie Jr., Temporal evolution of the deep western boundary current where it enters the sub-tropical domain, *Deep Sea Res*., *Ser. I*, *45*, 1053–1083, 1998.

Pierce, D. W., T. P. Barnett, and U. Mikolajewicz, Competing roles of heat and freshwater flux in forcing thermohaline oscillations, *J. Phys. Oceanogr*., *25*, 2046–2064, 1995.

Rahmstorf, S., and M. H. England, Influence of Southern Hemisphere winds on North Atlantic Deep Water flow, *J. Phys. Oceanogr*., *27*, 2040–2054, 1997.

Reid, J. L., On the circulation of the South Atlantic Ocean, in *The South Atlantic: Present and Past Circulation*, edited by G. Wefer et al., pp. 13–44, Springer-Verlag, New York, 1996.

Sloyan, B. M., and S. R. Rintoul, The Southern Ocean limb of the global deep overturning circulation, *J. Phys. Oceanogr*., *31*, 143–173, 2001.

Stössel, A., On the impact of sea ice in a global ocean circulation model, *Ann. Glaciol*., *25*, 111–115, 1997.

Stössel, A., and S.-J. Kim, An interannual Antarctic sea-ice–ocean mode, *Geophys. Res. Lett*., *25*, 1007–1010, 1998.

Stössel, A., S.-J. Kim, and S. S. Drijfhout, The impact of Southern Ocean sea ice in a global ocean model, *J. Phys. Oceanogr*., *28*, 1999–2018, 1998.

Stramma, L., and M. England, On the water masses and mean circulation of the South Atlantic Ocean, *J. Geophys. Res*., *104*, 20,863–20,883, 1999.

Sy, A., M. Rhein, J. R. N. Lazier, K. P. Koltermann, J. Meincke, A. Putzka, and M. Bersch, Surprisingly rapid spreading of newly formed intermediate waters across the North Atlantic Ocean, *Nature*, *386*, 675–679, 1997.

Turrell, W. R., G. Slesser, R. D. Adams, R. Payne, and P. A. Gillibrand, Decadal variability in the composition of Faroe Shetland Channel bottom water, *Deep Sea Res*., *Ser. I*, *46*, 1–25, 1999.

Whitworth, T., III, W. D. Nowlin Jr., R. D. Pillsbury, M. I. Moore, and R. F. Weiss, Observations of the Antarctic Circumpolar Current and deep boundary current in the southwest Atlantic, *J. Geophys. Res*., *96*, 15,105–15,118, 1991.

Whitworth, T., A. H. Orsi, S.-J. Kim, W. D. Nowlin, and R. A. Locarnini, Water masses and mixing near the Antarctic slope front, in *Ocean, Ice, and Atmosphere: Interactions at the Antarctic Continental Margin*, *Antarct. Res. Ser*., vol. 75, edited by S. S. Jacobs and R. F. Weiss, pp. 1–27, AGU, Washington, D. C., 1998.

Wolff, J.-O., E. Maier-Reimer, and S. Legutke, The Hamburg Ocean Primitive Equation model HOPE, *Tech. Rep. 13*, German Clim. Comput. Cent., Hamburg, Germany, 1997.

Woodruff, S. D., R. J. Slutz, R. L. Jenne, and P. M. Streurer, A comprehensive ocean-atmosphere data set, *Bull. Am. Meteorol. Soc*., *68*, 1239–1250, 1987.

Zangenberg, N., and G. Siedler, Path of the North Atlantic Deep Water in the Brazil Basin, *J. Geophys. Res*., *103*, 5419–5428, 1998.

Zenk, W., and N. G. Hogg, Warming trend in Antarctic Bottom Water flowing into the Brazil Basin, *Deep Sea Res*., *Ser. I*, *43*, 1461–1473, 1996.

Zenk, W., G. Siedler, B. Lenz, and N. G. Hogg, Antarctic Bottom Water flow through the Hunter Channel, *J. Phys. Oceanogr*., *29*, 2785–2801, 1999.

S.-J. Kim, Canadian Center for Climate Modelling and Analysis, University of Victoria, 3964 Gordon Head Road, Victoria, British Columbia, Canada V8N 3X3. (Seong-Joong.Kim@ec.gc.ca)

A. Stössel, Department of Oceanography, Texas A&M University, Texas Center for Climate Studies, College Station, TX 77843-3146, USA. (achim@advect.tamu.edu)

(Received March 27, 2000; revised May 15, 2001;
accepted June 11, 2001.)